

## Supporting information

### **Simultaneous enhancement in charge separation and onset potential for water oxidation in BiVO<sub>4</sub> photoanode by W-Ti codoping**

Xin Zhao,<sup>a†</sup> Jun Hu,<sup>a,e†</sup> Bo Wu,<sup>b</sup> Amitava Banerjee,<sup>c</sup> Sudip Chakraborty,<sup>c\*</sup> Jianyong Feng,<sup>a</sup>

Zongyan Zhao,<sup>f</sup> Shi Chen,<sup>b</sup> Rajeev Ahuja,<sup>c,d</sup> Tze Chien Sum,<sup>b\*</sup> Zhong Chen<sup>a\*</sup>

<sup>a</sup>*School of Materials Science and Engineering, Nanyang Technological University, 50 Nanyang Avenue, 639798, Singapore, Singapore.*

<sup>b</sup>*School of Physical and Mathematical Sciences, Nanyang Technological University, 637371, Singapore, Singapore*

<sup>c</sup>*Materials Theory Division, Department of Physics and Astronomy, Uppsala University, 75120, Sweden*

<sup>d</sup>*Applied Materials Physics, Department of Materials and Engineering, Royal Institute of Technology (KTH), S-100 44 Stockholm, Sweden*

<sup>e</sup>*School of Chemical Engineering, Northwest University, Xi'an, P. R. China 710069*

<sup>f</sup>*Faculty of Materials Science and Engineering, Kunming University of Science and Technology, Kunming 650093, P. R. China*

\*E-mail: [ASZChen@ntu.edu.sg](mailto:ASZChen@ntu.edu.sg)

†Dual contributors

## Computational Methodology:

We have carried out density functional theory (DFT) based electronic structure calculations to investigate the energetics and optical responses of experimentally synthesized 2% W and Ti co-doped monoclinic BiVO<sub>4</sub> of sheelite type structure. W and Ti were supposed to replace V sites instead of Bi sites, on the basis of the reported work that V site substitution has a smaller formation energy.<sup>1</sup> Projector augmented wave (PAW) formalism implemented VASP (Vienna Ab-initio Simulation Package) program has been used throughout the calculations,<sup>2,3</sup> to simulate the optical absorption cross-section. The core electrons behaviour and the interaction between valence electrons and the ion can be described properly in the PAW approach. The Perdew-Burke-Ernzerhof (PBE) form of generalized gradient approximation (GGA) has been employed as the exchange-correlation functional to obtain the optimized configuration of pristine and W and Ti co-doped BiVO<sub>4</sub> and consequently the respective optical absorption cross-section.<sup>4</sup> The Brillouin zone has been sampled by 3×3×3 Monkhorst Pack scheme of k-points. The energy cut-off of the plane wave basis set describing the valence electrons has been set at 520 eV after energy convergence check. To calculate the optical absorption cross-section, we have increased the number of bands as double of the initial one so that there will be enough number of unoccupied states for allowed HOMO-LUMO transitions. For determining the Density of States, the k-points have been doubled of the initial k-points. The structure has been optimized until the calculate Hellman-Feynman forces are smaller than 0.01eV/Å.

The frequency dependent dielectric function  $\varepsilon(\omega) = \varepsilon_1(\omega) + i\varepsilon_2(\omega)$  has been calculated. The imaginary part of the dielectric function can be derived from the Fermi golden rule, which is eventually turns as the optical absorption cross section:

$$\varepsilon_2(\omega) = \frac{4\pi^2 e^2}{\Omega} \lim_{q \rightarrow 0} \frac{1}{q^2} \sum_{c,v,k} 2w_k \delta(\varepsilon_{ck} - \varepsilon_{vk} - \omega) \times \langle \mu_{ck+e_{\alpha}q} | \mu_{vk} \rangle \langle \mu_{ck+e_{\beta}q} | \mu_{vk} \rangle^* \quad (1)$$

where the indices  $c$  and  $v$  refer to conduction and valence band states respectively, and  $\mu_{ck}$  is the cell periodic part of the electronic wave functions at a specific  $k$ -point.

A  $2 \times 2$  supercell of W doped  $\text{BiVO}_4$  (010) surface with a vacuum region of  $15 \text{ \AA}$  was chosen to investigate the surface property. The (010) surface was used because it is the most stable surface under the realistic conditions.<sup>5-7</sup> During the calculation, self-consistent periodic Density Functional Theory (DFT) calculations were employed. The Generalized Gradient Approximation (GGA), in the form of the Perdew-Burke-Ernzerhof (PBE) approximation was used to calculate the exchange-correlation energy. The Broyden-Fletcher-Goldfarb-Shanno (BFGS) scheme was chosen as the minimization algorithm. DFT-D correction was applied during the dispersion corrections. Hubbard U-corrections to the d electrons of V (LDA+U, effective  $U(\text{V})=2.5 \text{ eV}$ ) and spin-polarization were performed during the calculations. Ultrasoft pseudopotentials in reciprocal space were used, where the electron configuration of the valence was set as O- $2s^2 2p^4$ , Ti- $3s^2 3p^6 3d^2 4s^2$ , V- $3p^6 3d^3 4s^2$ , W- $5p^6 5d^4 6s^2$ , and Bi- $5d^{10} 6s^2 6p^3$ . Gaussian smearing scheme with the smearing width of  $0.05 \text{ eV}$  with 30% empty band was applied in the calculation. The external stress and hydrostatic pressure were set at  $0 \text{ GPa}$ . The energy cutoff was set at  $380 \text{ eV}$  and the SCF tolerance  $1.0 \times 10^{-6} \text{ eV/atom}$ . The convergence criteria for the structure optimization and energy calculation were set to an energy tolerance of  $5.0 \times 10^{-6} \text{ eV/atom}$ , a maximum force tolerance of  $0.01 \text{ eV/ \AA}$ ,  $0.02 \text{ GPa}$  and a maximum displacement tolerance of  $5.0 \times 10^{-4} \text{ \AA}$ , respectively.  $2 \times 1 \times 1$  k-points sampling was used for the surface calculations. The Fermi level is simply defined as the valence band maximum (VBM) for n-type semiconductors and insulators in the CASTEP code and some other codes.<sup>8,9</sup>

### **Adsorption and surface energies calculation.**

The adsorption energy ( $E_{\text{ads}}$ ) between surface and adsorbed particles was computed by equation

2.

$$E_{\text{ads}} = E_{\text{molecule+surface}} - E_{\text{molecule}} - E_{\text{surface}} \quad (2)$$

“where  $E_{\text{molecule+surface}}$  is the total energy of the system, including the adsorption molecules and the  $\text{BiVO}_4$  facet;  $E_{\text{molecule}}$  is the optimized energy of adsorption molecules, which can be derived from the reference species including  $\text{H}_2\text{O}$  and  $\text{H}_2$ . For example,  $E_{\text{OH}^-} = E_{\text{H}_2\text{O}} - 0.5E_{\text{H}_2}$ . The energy of  $\text{H}_2\text{O}$  and  $\text{H}_2$  are -468.71 eV and -31.55 eV respectively.<sup>10</sup>  $E_{\text{surface}}$  is the energy of  $\text{BiVO}_4$  facet.” In the definitions, the higher negative value of  $E_{\text{ads}}$  indicates a more stable adsorption on the plane. All the calculated energies reported herein include Zero-Point Energy (ZPE) correction.<sup>11</sup> The surface energy ( $\gamma$ ) can be calculated by the following equation 3:

$$\gamma = \frac{1}{2A} (E_{\text{slab}} - nE_{\text{bulk}}) \quad (3)$$

where  $E_{\text{slab}}$  is the total energy of the slab model,  $E_{\text{bulk}}$  is the total energy per unit cell of the bulk,  $n$  is the number of unit cells that the slab model contains, and  $A$  is the surface area of the slab model.

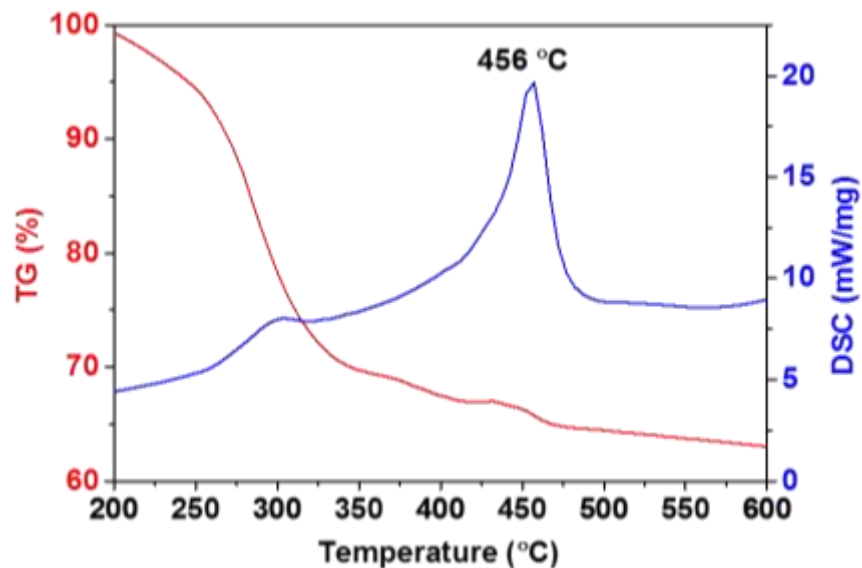


Fig. S1 TG-DTA curves of the transparent gel dried at 120°C.

Fig. S1 shows TG-DTA curves of the dried gel. 3 stages of weight loss were observed at below 250 °C, 250-330 °C and 330-600 °C in the TG curve. The first weight loss might come from the evaporation of ethylene glycol in the gel. The following sharp weight loss is due to the combustion of resultant organics in the gel, corresponding to an exothermic peak at around 300 °C. The third weight loss is the removal of the residual organic components and reaction of the inorganic components to form  $\text{BiVO}_4$ . A corresponding exothermic peak at 456 °C was observed, which is the formation temperature of  $\text{BiVO}_4$ . Thus, in this study, we take 500 °C as the sample preparation temperature to ensure complete formation of  $\text{BiVO}_4$ .

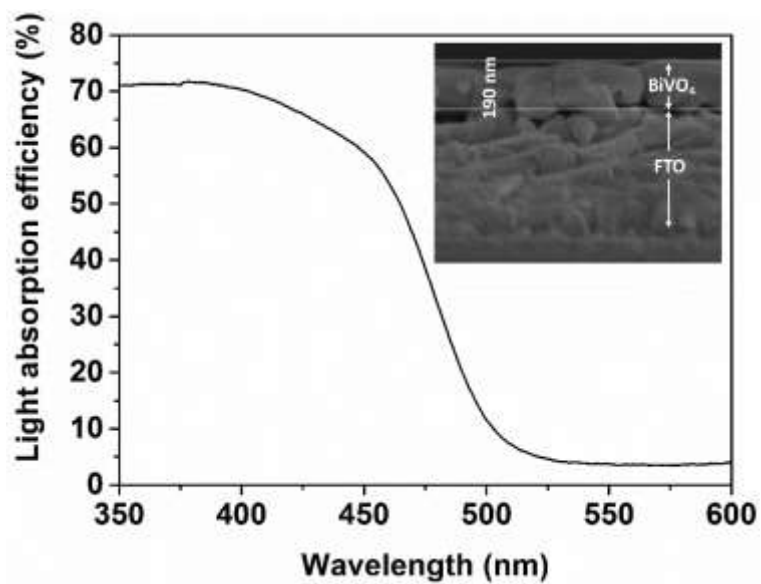


Fig. S2 Light absorption efficiency of pristine BiVO<sub>4</sub>.

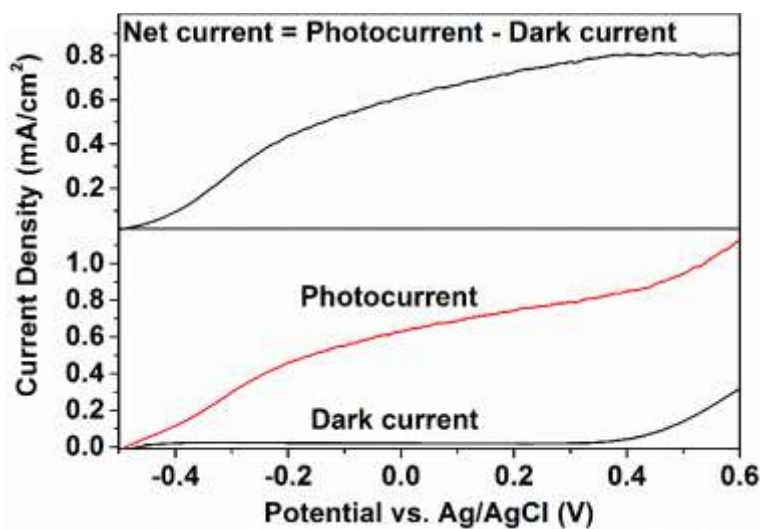


Fig. S3 Photocurrent of pristine BiVO<sub>4</sub> with 0.1 M Na<sub>2</sub>SO<sub>3</sub>.

### **Analysis for the front and back illumination photocurrent**

For front-side illumination, the photo-excited carriers are generated mostly near the BiVO<sub>4</sub>-electrolyte interface region. Thus, electron will transport a relatively long path to the FTO before reaching the counter electrode, while hole travels a relatively short distance to the electrolyte. On the contrary, from the back side illumination, the photo-excited carriers are mostly generate near the FTO-BiVO<sub>4</sub> interface region. Thus, electron will transport a relatively short path to the FTO, while hole travels a relatively a longer distance to the electrolyte. Hence, Front and back illumination photocurrents can reflect the relative transport property of electron and hole. Higher front illumination photocurrent indicates better electron transport. Otherwise, higher back illumination photocurrent indicates better hole transport.

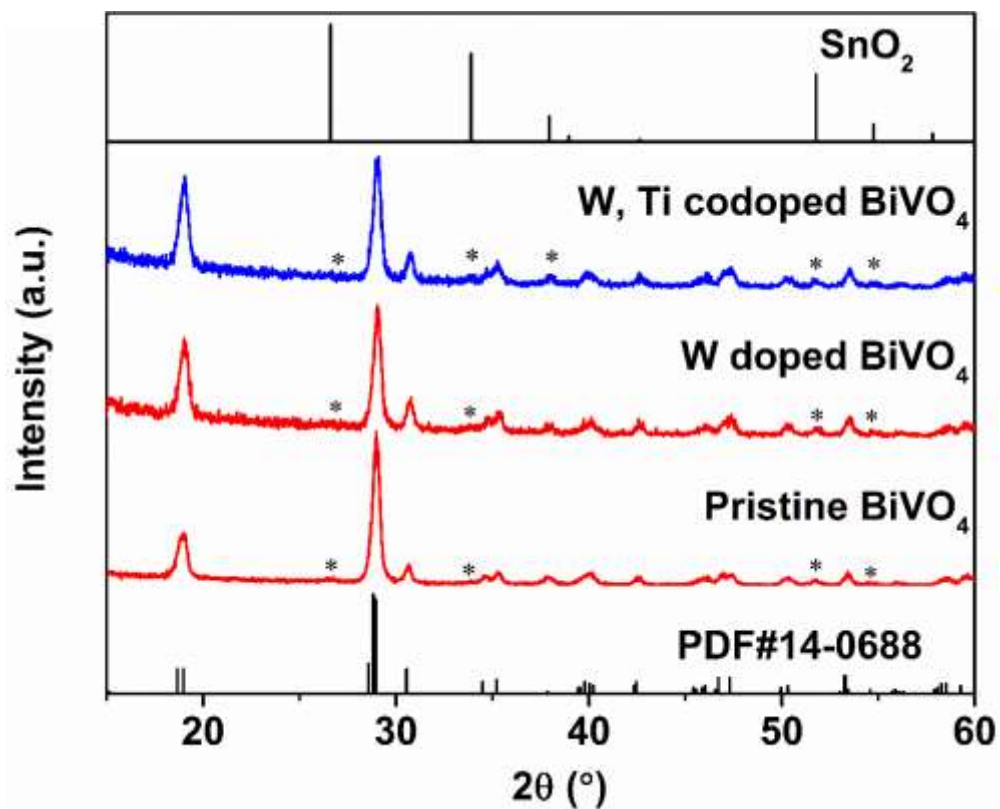


Fig. S4 X-ray diffraction patterns of pristine, W doped  $\text{BiVO}_4$  and W-Ti codoped  $\text{BiVO}_4$ .

Peaks from FTO substrates have been mark with \*.

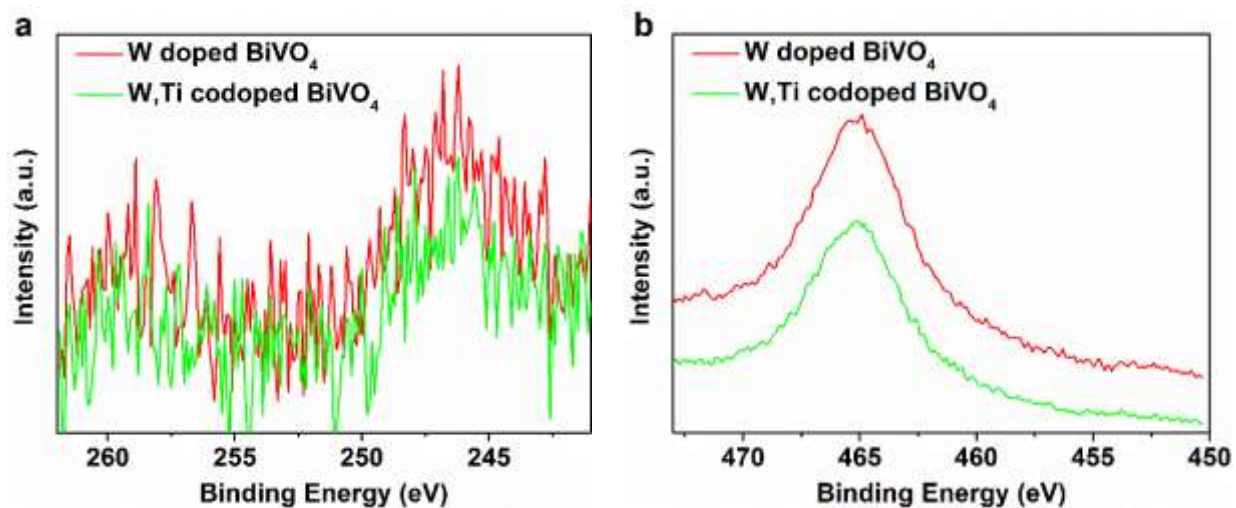




Fig. S5 (a) W 4d and (b) Ti 2p core-level X-ray photoelectron spectroscopy (XPS) of W doped BiVO<sub>4</sub> and W-Ti codoped BiVO<sub>4</sub>.

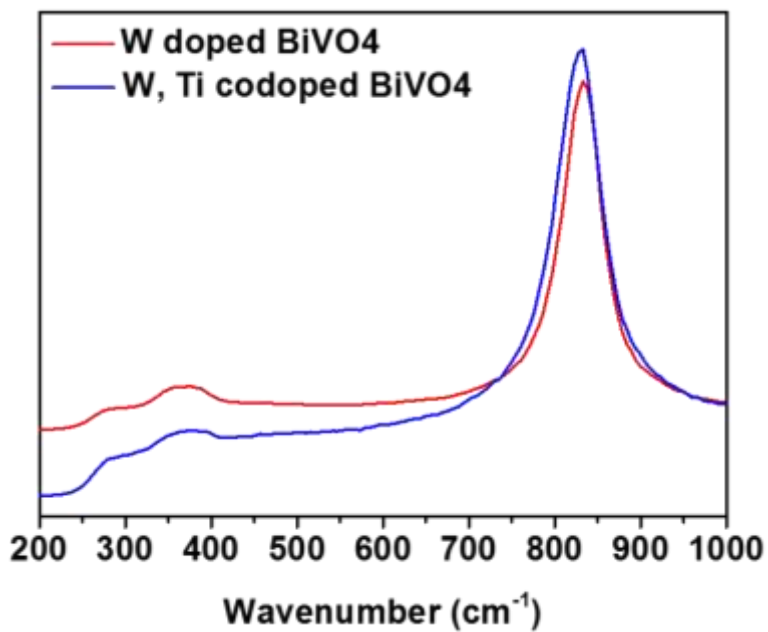


Fig. S6 Raman spectra for W doped BiVO<sub>4</sub> and W-Ti codoped BiVO<sub>4</sub>.

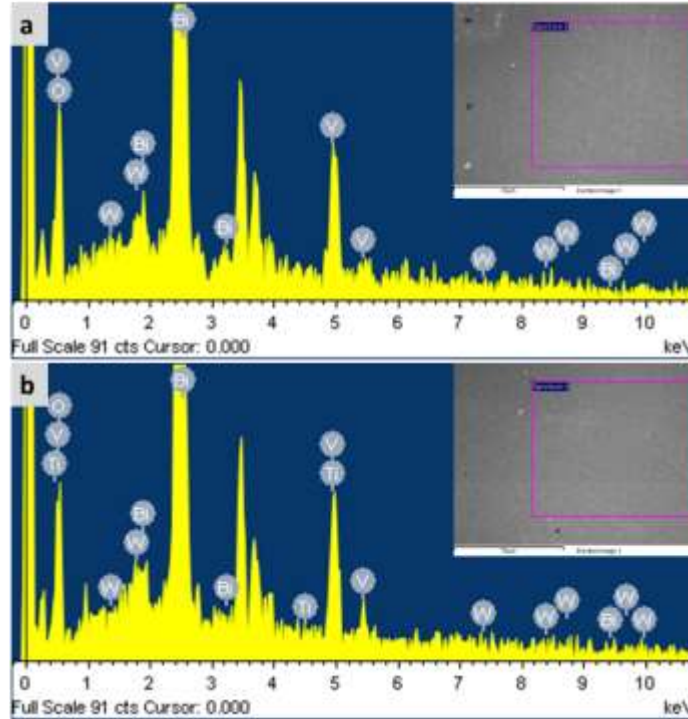


Fig. S7 EDX of (a) W doped BiVO<sub>4</sub> and (b) W-Ti codoped BiVO<sub>4</sub>.

**Table S1 Energetics and Volume changes of pristine and doped BiVO<sub>4</sub> based on DFT calculations.**

Structure	Total Energy (eV) [eV/atom]	Energy Difference (%) vs Pristine	Total Volume (Å <sup>3</sup> )	Volume Difference (%) vs Pristine	Volume Difference (%) vs BiVO <sub>4</sub> +2%W
Pristine BiVO <sub>4</sub>	-707.225 [-7.36]		1255.08		
BiVO <sub>4</sub> +2% W	-710.119 [-7.39]	0.41	1261.70	0.53	

BiVO <sub>4</sub> +2%	-710.761	0.49	1265.85	0.86	0.33
(W+Ti)	[-7.40]				

In this study, we employed sol-gel method to prepare BiVO<sub>4</sub> thin films for facile doping of different elements. X-ray diffraction shows all peaks of pristine, W doped BiVO<sub>4</sub> and W-Ti codoped BiVO<sub>4</sub> agree well with monoclinic BiVO<sub>4</sub> without any other impurity phases (Fig. S3). This demonstrates monoclinic BiVO<sub>4</sub> thin film can be easily synthesized by this sol-gel method. Moreover, this method is facile for doping mono or multiple elements. XPS were tested to verify the doping (Fig. S4). However, only W can be identified in the XPS spectra. Ti signal overlaps with the signal of Bi 4d<sub>3/2</sub> at around 465eV, thus, only a broad peak of Bi 4d<sub>3/2</sub> was observed. Many reported XPS wide scan indicate such a peak at around 465 eV.<sup>12, 13</sup> Due to the large peak intensity of this peak, our capability to resolve Ti 2p<sub>3/2</sub> peak is greatly reduced. Raman was then used to characterize Ti doping. W doped BiVO<sub>4</sub> was as the reference in the analysis. Fig. S5 shows the Raman spectra for W doped BiVO<sub>4</sub> and W-Ti codoped BiVO<sub>4</sub>. The strongest peak at 833 cm<sup>-1</sup> of W doped BiVO<sub>4</sub> is attributed to the symmetric stretching modes of VO<sub>4</sub> tetrahedra.<sup>14, 15</sup> With codoping Ti, a marginal shift appears in the VO<sub>4</sub> tetrahedra vibration, which indicates Ti is incorporated into BiVO<sub>4</sub> lattice occupying the V site. Though the shift is small, the results is highly repeatable and consistent with the reported results by Mullins et al, in which a slight shift in Raman was also observed after doping Mo or W into BiVO<sub>4</sub> single crystal.<sup>16</sup> Moreover, we also considered the formation of the doping from theoretical view. The formation energies were given in Table S1. It is found that W mono doping or W-Ti codoping are not difficult, formation energies of which are

close to that of pristine one. And in experiment a lot of research work has reported the W doped  $\text{BiVO}_4$  and great enhancement has been observed due to the enhanced electron density, which suggests that W can be easily doped into  $\text{BiVO}_4$ .<sup>17, 18</sup> Since W-Ti codoping has a quite similar formation energy with mono W doping, it is reasonable to believe that W-Ti can also be doped into  $\text{BiVO}_4$ . Elemental information was also analyzed by Energy-dispersive X-ray spectroscopy (EDS), which showed that W concentration was around 2.8 at% in W-doped  $\text{BiVO}_4$  and Ti and W concentrations were 3.2 at% and 3.3 at% respectively in W-Ti codoped  $\text{BiVO}_4$  (Fig. S6).

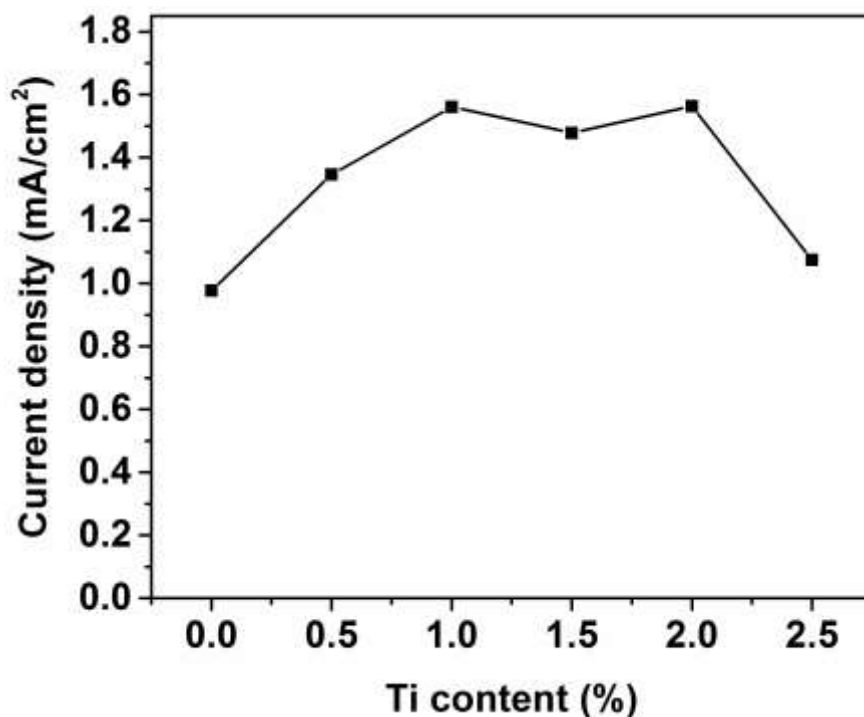


Fig. S8 The photocurrent at 1.23 V vs. RHE of nominal 2 at% W doped  $\text{BiVO}_4$  codoped with different amount of Ti.

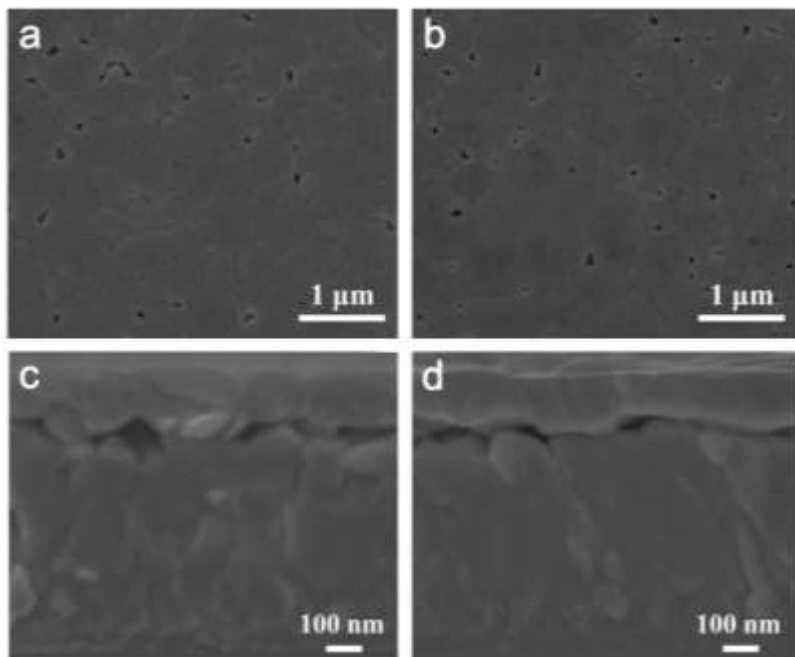


Fig. S9 Top view SEM images of (a) W doped BiVO<sub>4</sub> film and (b) W-Ti codoped BiVO<sub>4</sub> film. Cross-section SEM images of (c) W doped BiVO<sub>4</sub> film and (d) W-Ti codoped BiVO<sub>4</sub> film.

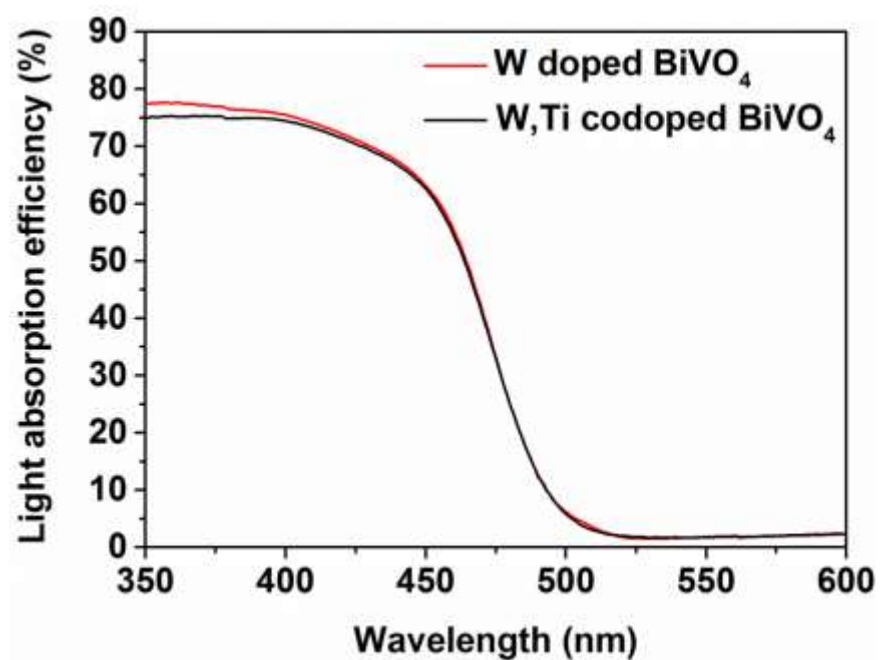


Fig. S10 Light absorption efficiency of W doped BiVO<sub>4</sub> and W-Ti codoped BiVO<sub>4</sub> films.

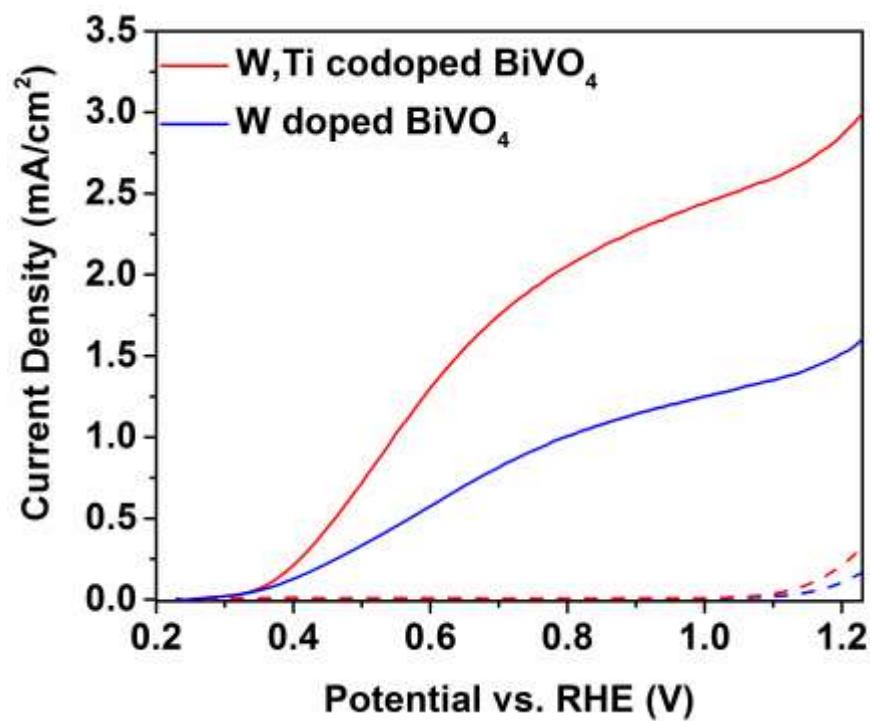


Fig. S11 Photocurrents of W doped BiVO<sub>4</sub> and W-Ti codoped BiVO<sub>4</sub> films under AM1.5G illumination with hole scavenger Na<sub>2</sub>SO<sub>3</sub>. Dark currents were shown in dash lines.

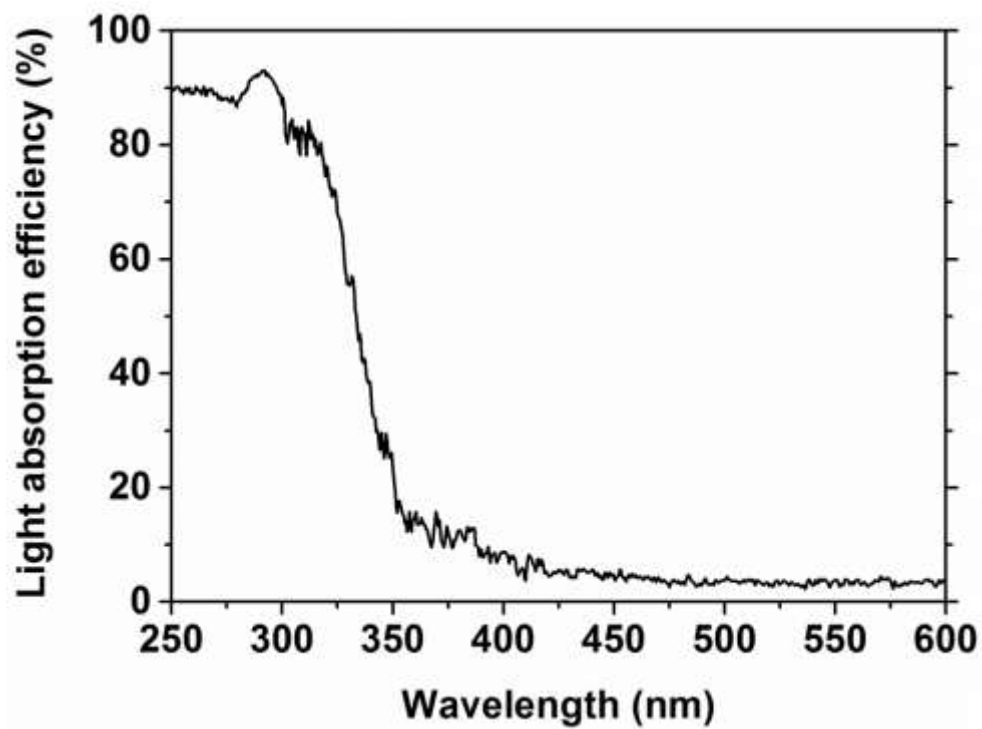


Fig. S12 Light absorption efficiency of FTO.

**Effective Mass Calculations:**

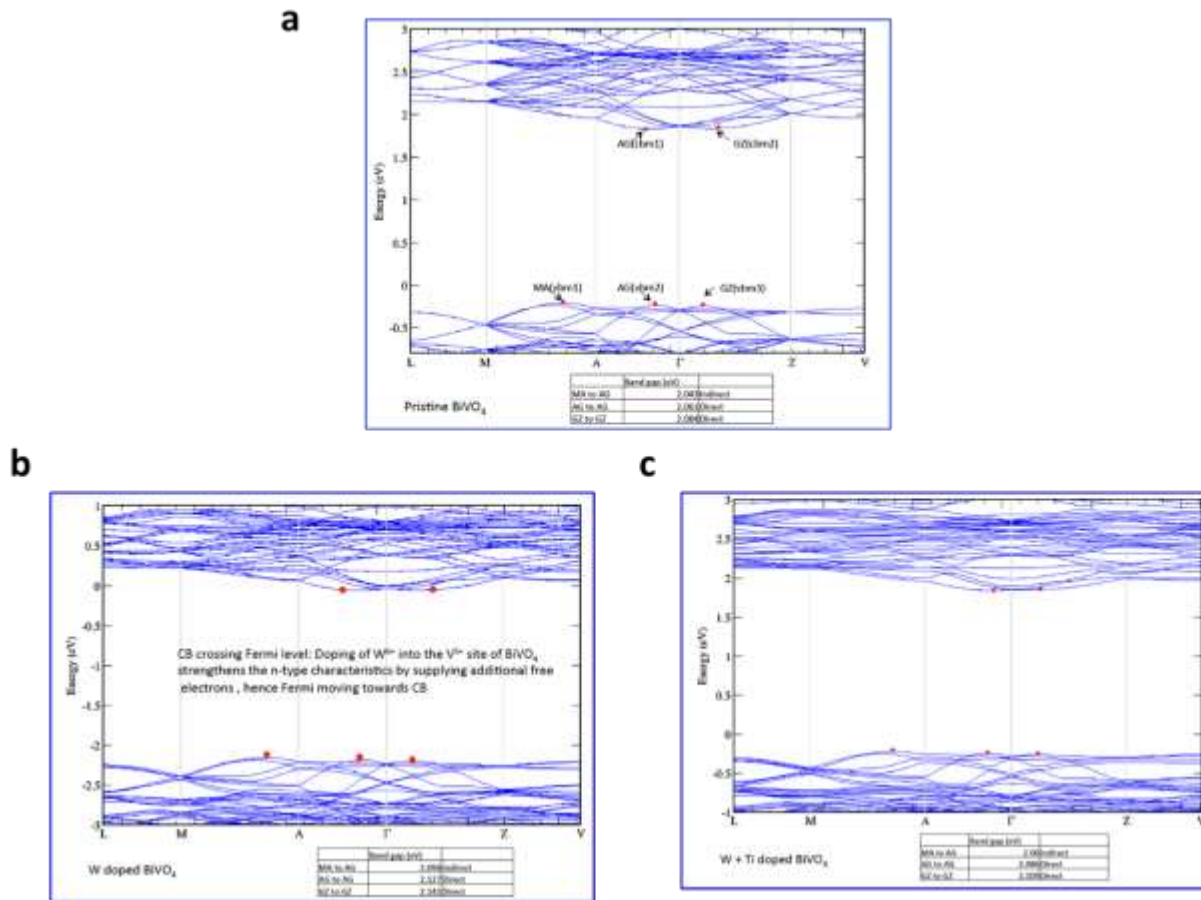


Fig. S13 Band structure for calculation of the effective mass (a) pristine  $\text{BiVO}_4$ , (b) W doped  $\text{BiVO}_4$ , and (c) W-Ti codoped  $\text{BiVO}_4$ .



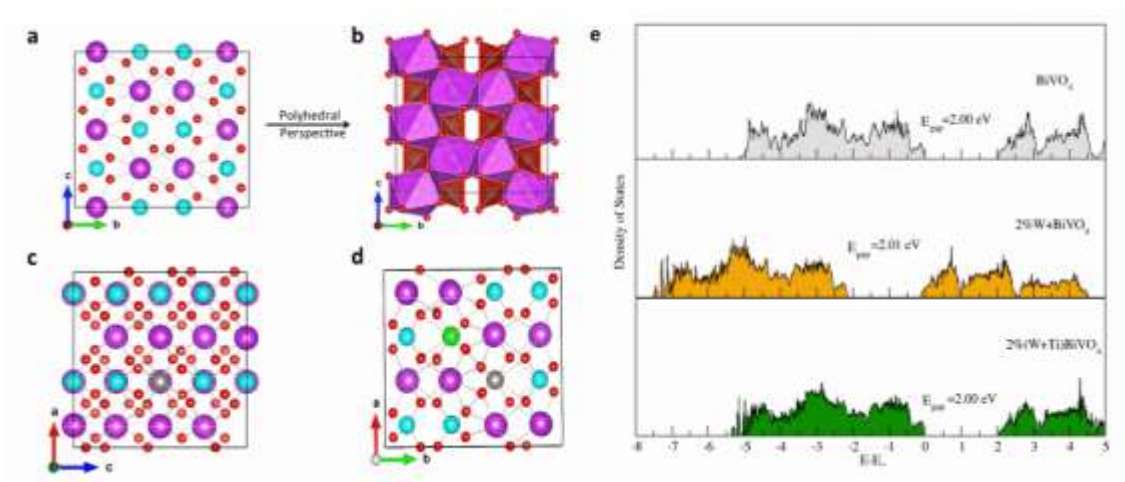


Fig. S14 Crystal Structure of (a) pristine, (c) W-doped and (d) W-Ti co-doped  $\text{BiVO}_4$ . (b) Polyhedra perspective of pristine  $\text{BiVO}_4$ .  $\text{BiO}_8$  polyhedra has been represented by magenta color. Bi, V, O, W, Ti are represented by magenta, blue, red, grey and green colours. (e) DOS of pristine and doped  $\text{BiVO}_4$ .

Monoclinic  $\text{BiVO}_4$  possesses a layered structure of alternate arrangement of Bi and V cation, along the crystallographic c axis (Fig. S13a). In monoclinic  $\text{BiVO}_4$ , two polyhedra units,  $\text{VO}_4$  tetrahedra (red polyhedra in Fig. S13b) and  $\text{BiO}_8$  dodecahedra (magenta polyhedra in Fig. S13b) linked to each other by edge sharing. The distortions of these two polyhedra create even number (2 and 4) of oxygen neighbour of tetrahedra and dodecahedra, respectively. The substitution of V by W (Fig. S13c) and also co-doping of W-Ti (Fig. S13d) increase the cell volume of pristine  $\text{BiVO}_4$  by 0.53% and 0.86 % respectively. This change in volume can be attributed to the volume of doped polyhedra that induces distortion in the neighbouring polyhedra. Doping with W creates volume change in  $\text{VO}_4$  polyhedra on the order of  $+0.1\text{-}0.2\text{\AA}^3$  and in  $\text{BiO}_8$  polyhedra  $+0.3\text{-}0.8\text{\AA}^3$ . Similar phenomenon is also observed in case of co-doped W-Ti system, with a higher degree of distortion than W doping, which leads to a higher volume change. It is worth mentioning that the

energy change (total and energy/atom) of the system (as depicted in Table S1) leads to a higher stability with W doping and W-Ti codoping.

Fig. S13e shows the density of states of pristine, W-doped  $\text{BiVO}_4$  and W-Ti codoped  $\text{BiVO}_4$ . Mono and co-doping with W and W-Ti have no much impact on the band gap of pristine  $\text{BiVO}_4$  of around 2.0 eV, which is consistent with the light absorption measurement (Fig. S10). Meanwhile, comparing W mono and W-Ti codoping, there is a very small change in band gap (0.01 eV), which agrees well with the hole absorption peak in Fig. 3c in the main text.

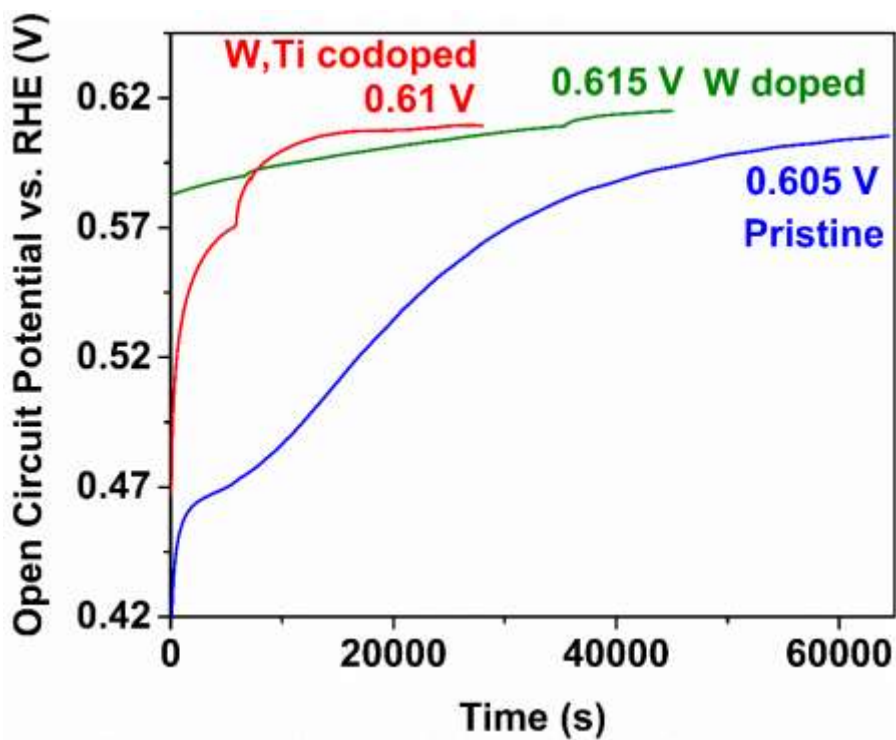


Fig. S15 Open circuit potentials of pristine, W doped, W-Ti codoped  $\text{BiVO}_4$ .

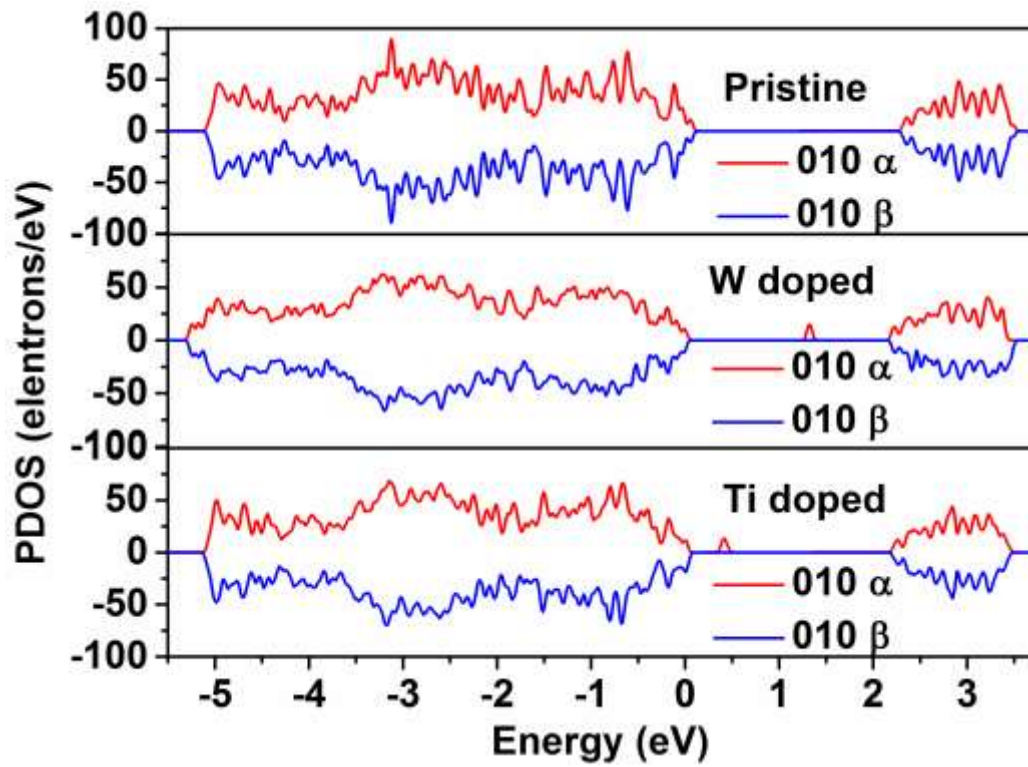


Fig. S16 The  $\alpha$  and  $\beta$  orbits of pristine, W doped, W-Ti codoped and Ti doped BiVO<sub>4</sub> (010) facets.

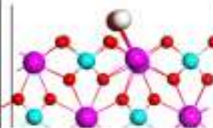

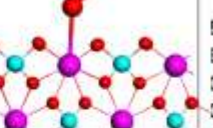
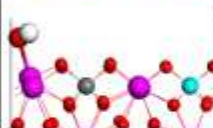


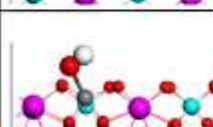
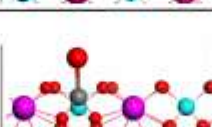
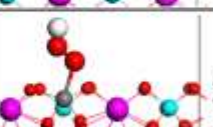
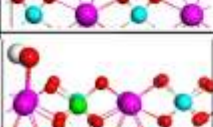
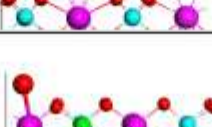
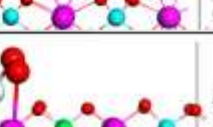
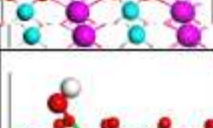
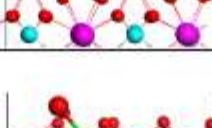
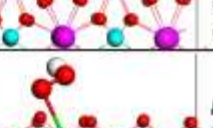
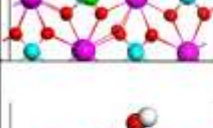
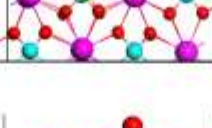
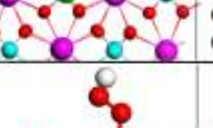
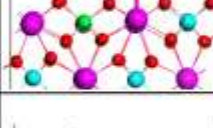
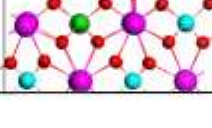
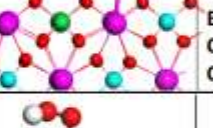
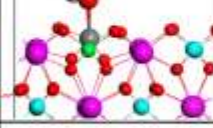
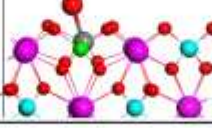
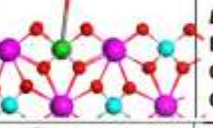
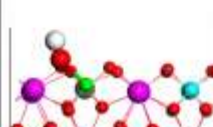


		@ OH <sub>ads</sub>	@ O <sub>ads</sub>	@ OOH <sub>ads</sub>
Pristine	Bi site	 $E_{ads}=-0.90$ ; Bi-O=2.14; O-H=0.99	 $E_{ads}=-1.44$ Bi-O=2.20	 $E_{ads}=-0.25$ Bi-O <sub>1</sub> =2.80 O <sub>1</sub> -O <sub>2</sub> =1.35 O <sub>2</sub> -H=1.00
	W site	 $E_{ads}=-2.49$ Bi-O=2.08 O-H=0.98	 $E_{ads}=-2.60$ Bi-O=2.13	 $E_{ads}=-0.82$ Bi-O <sub>1</sub> =2.15 O <sub>1</sub> -O <sub>2</sub> =1.46 O <sub>2</sub> -H=0.98
W doped	Bi site	 $E_{ads}=-2.46$ W-O=1.98 O-H=0.98	 $E_{ads}=-3.06$ W-O=1.85	 $E_{ads}=-0.95$ W-O <sub>1</sub> =1.98 O <sub>1</sub> -O <sub>2</sub> =1.46 O <sub>2</sub> -H=0.99
	W site	 $E_{ads}=-1.18$ Bi-O=2.09 O-H=0.99	 $E_{ads}=-1.59$ Bi-O=2.07	 $E_{ads}=-0.81$ Bi-O <sub>1</sub> =2.68 O <sub>1</sub> -O <sub>2</sub> =1.34 O <sub>2</sub> -H=1.02
Ti doped	Bi site	 $E_{ads}=-2.14$ Bi-O=2.58 O-H=0.99	 $E_{ads}=-3.93$ Bi-O=2.08	 $E_{ads}=-1.05$ Bi-O <sub>1</sub> =2.89 O <sub>1</sub> -O <sub>2</sub> =1.45 O <sub>2</sub> -H=0.99
	Ti site	 $E_{ads}=-0.83$ Bi-O=2.14 O-H=0.99	 $E_{ads}=-1.26$ Bi-O=2.20	 $E_{ads}=-0.21$ Bi-O <sub>1</sub> =2.84 O <sub>1</sub> -O <sub>2</sub> =1.35 O <sub>2</sub> -H=0.99
TiW doped	Bi site	 $E_{ads}=-0.68$ Bi-O=1.93 O-H=0.99	 $E_{ads}=-2.41$ Bi-O=1.91	 $E_{ads}=0.02$ Bi-O <sub>1</sub> =3.97 O <sub>1</sub> -O <sub>2</sub> =1.35 O <sub>2</sub> -H=1.00
	W site	 $E_{ads}=-1.33$ Bi-O=2.01 O-H=0.98	 $E_{ads}=-1.41$ Bi-O=1.88	 $E_{ads}=-0.02$ Bi-O <sub>1</sub> =3.69 O <sub>1</sub> -O <sub>2</sub> =1.35 O <sub>2</sub> -H=1.00
	Ti site	 $E_{ads}=-1.33$ Bi-O=2.01 O-H=0.98	 $E_{ads}=-1.41$ Bi-O=1.88	 $E_{ads}=-0.02$ Bi-O <sub>1</sub> =3.69 O <sub>1</sub> -O <sub>2</sub> =1.35 O <sub>2</sub> -H=1.00

Fig. S17. The adsorption structures and energies of OH<sub>ads</sub>, O<sub>ads</sub> and OOH<sub>ads</sub> involved in a water splitting process on clean, W doped and Ti doped BiVO<sub>4</sub> (010) facets. The unit of bond length is Å and the adsorption energy is eV. The “@” signs stand for adsorption state on the facet.

Thermodynamics of the chemical reaction are calculated in four steps. The first step is the one that adsorbed H<sub>2</sub>O moiety is dissociated at the active sites with the interaction of the photo-generated surface hole. A surface hole ( $h^+$ ) reacts with an adsorbed H<sub>2</sub>O to release a proton and creates an OH<sub>ads</sub> radical. Then, the OH<sub>ads</sub> will release another H adatom to generate an O adatom. This process will consume more energy due to the high positive value of Gibbs energy change ( $\Delta G$ ). After that, the generated O adatom is extremely electrophilic and immediately obtains an electron by bonding to an adjacent H<sub>2</sub>O. The last step is O-O separation from surface with the help of potential bias. Researches indicated that the V atom is not an active site because it cannot be further oxidized on a perfect surface.<sup>19, 20</sup> Thus, V site is not considered for calculation of adsorption of reacting species. Fig. S15 illustrates detailed information about the adsorption of several key species on different sites. As indicated, the adsorption energies of OH<sub>ads</sub> on Bi atom are -0.90 eV, -2.49 eV and -1.18 eV for clean, W doped and Ti doped BiVO<sub>4</sub> (010) facets respectively. Therefore, the doped surface can greatly improve the adsorption ability especially for the W doped surface. Furthermore, doped atoms in the surface can also adsorb the species, indicating the doped atoms may be the active sites on the surface.

## References

1. W.-J. Yin, S.-H. Wei, M. M. Al-Jassim, J. Turner and Y. Yan, *Phys. Rev. B*, 2011, **83**, 155102.
2. G. Kresse and J. Hafner, *Phys. Rev. B*, 1993, **47**, 558.
3. G. Kresse and J. Furthmüller, *Phys. Rev. B*, 1996, **54**, 11169.
4. J. P. Perdew, K. Burke and M. Ernzerhof, *Phys. Rev. Lett.*, 1996, **77**, 3865.
5. W. Luo, J. Wang, X. Zhao, Z. Zhao, Z. Li and Z. Zou, *Phys. Chem. Chem. Phys.*, 2013, **15**, 1006-1013.
6. J. Yang, D. Wang, X. Zhou and C. Li, *Chem. Eur. J.*, 2013, **19**, 1320-1326.
7. Z. Zhao, Z. Li and Z. Zou, *RSC Adv.*, 2011, **1**, 874-883.
8. W. Liu, W. Zheng and Q. Jiang, *Phys. Rev. B* 2007, **75**, 235322.
9. B. Engels, P. Richard, K. Schroeder, S. Blügel, P. Ebert and K. Urban, *Phys. Rev. B*, 1998, **58**, 7799.
10. J. Hu, W. Chen, X. Zhao, H. Su and Z. Chen, *ACS Appl. Mater. Interfaces*, 2018, **10**, 5475-5484.
11. Z.-Q. Huang, B. Long and C.-R. Chang, *Catal. Sci. Technol.*, 2015, **5**, 2935-2944.
12. Y. Q. Liang, T. Tsubota, L. P. A. Mooij and R. van de Krol, *J. Phys. Chem. C*, 2011, **115**, 17594-17598.
13. W. Luo, Z. Yang, Z. Li, J. Zhang, J. Liu, Z. Zhao, Z. Wang, S. Yan, T. Yu and Z. Zou, *Energy Environ. Sci.*, 2011, **4**, 4046-4051.
14. A. J. Rettie, H. C. Lee, L. G. Marshall, J.-F. Lin, C. Capan, J. Lindemuth, J. S. McCloy, J. Zhou, A. J. Bard and C. B. Mullins, *J. Am. Chem. Soc.*, 2013, **135**, 11389-11396.
15. F. F. Abdi, N. Firet and R. van de Krol, *ChemCatChem*, 2013, **5**, 490-496.
16. D. K. Zhong, S. Choi and D. R. Gamelin, *J. Am. Chem. Soc.*, 2011, **133**, 18370-18377.
17. J. Hu, X. Zhao, W. Chen, H. Su and Z. Chen, *J. Phys. Chem. C*, 2017, **121**, 18702-18709.
18. M. Oshikiri and M. Boero, *J. Phys. Chem. B*, 2006, **110**, 9188-9194.

1. W.-J. Yin, S.-H. Wei, M. M. Al-Jassim, J. Turner and Y. Yan, *Physical Review B*, 2011, **83**, 155102.
2. G. Kresse and J. Hafner, *Physical Review B*, 1993, **47**, 558.
3. G. Kresse and J. Furthmüller, *Physical review B*, 1996, **54**, 11169.
4. J. P. Perdew, K. Burke and M. Ernzerhof, *Physical review letters*, 1996, **77**, 3865.
5. W. Luo, J. Wang, X. Zhao, Z. Zhao, Z. Li and Z. Zou, *Physical Chemistry Chemical Physics*, 2013, **15**, 1006-1013.
6. J. Yang, D. Wang, X. Zhou and C. Li, *Chemistry-A European Journal*, 2013, **19**, 1320-1326.

7. Z. Zhao, Z. Li and Z. Zou, *RSC Advances*, 2011, **1**, 874-883.
8. W. Liu, W. Zheng and Q. Jiang, *Physical Review B*, 2007, **75**, 235322.
9. B. Engels, P. Richard, K. Schroeder, S. Blügel, P. Ebert and K. Urban, *Physical Review B*, 1998, **58**, 7799.
10. J. Hu, W. Chen, X. Zhao, H. Su and Z. Chen, *ACS Applied Materials & Interfaces*, 2018, **10**, 5475-5484.
11. Z.-Q. Huang, B. Long and C.-R. Chang, *Catalysis Science & Technology*, 2015, **5**, 2935-2944.
12. D.-K. Ma, M.-L. Guan, S.-S. Liu, Y.-Q. Zhang, C.-W. Zhang, Y.-X. He and S.-M. Huang, *Dalton Transactions*, 2012, **41**, 5581-5586.
13. Z. Sun, J. Guo, S. Zhu, J. Ma, Y. Liao and D. Zhang, *Rsc Advances*, 2014, **4**, 27963-27970.
14. Y. Q. Liang, T. Tsubota, L. P. A. Mooij and R. van de Krol, *J Phys Chem C*, 2011, **115**, 17594-17598.
15. W. Luo, Z. Yang, Z. Li, J. Zhang, J. Liu, Z. Zhao, Z. Wang, S. Yan, T. Yu and Z. Zou, *Energy & Environmental Science*, 2011, **4**, 4046-4051.
16. A. J. Rettie, H. C. Lee, L. G. Marshall, J.-F. Lin, C. Capan, J. Lindemuth, J. S. McCloy, J. Zhou, A. J. Bard and C. B. Mullins, *Journal of the American Chemical Society*, 2013, **135**, 11389-11396.
17. F. F. Abdi, N. Firet and R. van de Krol, *ChemCatChem*, 2013, **5**, 490-496.
18. D. K. Zhong, S. Choi and D. R. Gamelin, *Journal of the American Chemical Society*, 2011, **133**, 18370-18377.
19. J. Hu, X. Zhao, W. Chen, H. Su and Z. Chen, *The Journal of Physical Chemistry C*, 2017, **121**, 18702-18709.
20. M. Oshikiri and M. Boero, *The Journal of Physical Chemistry B*, 2006, **110**, 9188-9194.